PERGAMON

International Journal of Multiphase Flow 27 (2001) 617–634

International Journal of Multiphase Flow

www.elsevier.com/locate/ijmulflow

Shock waves attenuation by granular filters

A. Britan *, G. Ben-Dor, O. Igra, H. Shapiro

Department of Mechanical Engineering, Pearlstone Center for Aeronautical Engineering Studies, Ben-Gurion University of the Negev, 84105 Beer-Sheva, Israel

Received 17 January 2000; received in revised form 30 July 2000

Abstract

Proper design of protecting filters mitigates the effect of blast and shock waves and thereby makes such filters effective protection against both accidental and planned explosions. The main goal of the present study was to clarify the filter performance in reducing the loading on structures as well as reducing the strength of the transmitted shock. While most of the granular filters used for protection in the past were composed of sand or rock particles, in the present study the investigated granular filters were composed of small spherical particles. This was done in order to exclude the influence of the particle shape and to ease the numerical simulation of the filter performance. Moreover, in the simulations we neglected real effects such as particles movement and its rearrangement during the shock wave propagation and only discussion regarding the dependence of the granular filter performance on its length and composition is provided. Based on a comparison between experimental results and appropriate numerical simulations obtained for the pressure profiles inside and downstream of the filter it was found that the attenuation performance of the filter can be well predicted using a simple one-dimensional approach to the real, more complicated problems.

Keywords: Shock waves; Granular materials; Granular filters; Attenuation

1. Introduction

Direct exposure to shock or blast wave is harmful and therefore protective measures are needed. As an example let us view the case when a blast wave, generated by a high explosive weapon, hits the ground in a vicinity to a shelter as shown in Fig. 1. The unavoidable ventilation duct offers a way for the blast wave penetration into the shelter. It is a common practice to use a granular filter inside the air intake system to prevent such a penetration and to protect the expensive chemical filters placed in the bottom of the ventilation duct. While granular filters are

* Corresponding author.

0301-9322/01/$ - see front matter
PII: S0301-9322(00)00048-3

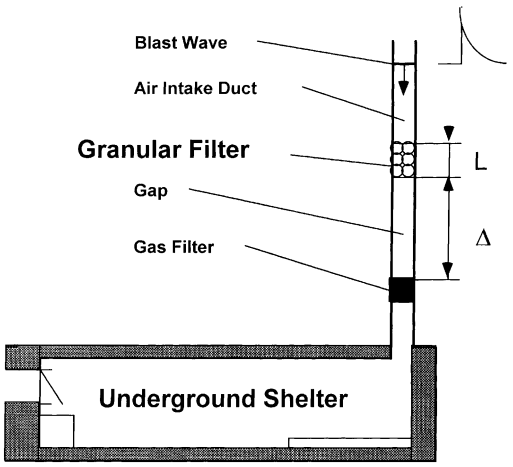

Fig. 1. Schematic drawing showing application of a granular filter.

widely used as protectors against shock and blast waves, very little information is available about their performance. Among the few available papers in this subject, the most relevant results are related to the attenuation of shock waves with a decaying pressure profile through the perforated partitions and grids; e.g. see Mori et al. (1975), Tong et al. (1980), Gelfand et al. (1987) and Lind et al. (1999). Note that the destructive nature of shock/blast waves depends upon the pressure signature of the incident shock as well as on the distance passed between the various obstacles. This makes the problem rather complex (Gelfand et al. 1987). Extensive measurements of the post shock wave overpressure upstream and downstream of various granular filters for shock waves with step-like pressure profiles were performed by Medvedev et al. (1990). The experimental results were compared with calculations and good agreement was found. Similar experiments were conducted recently by Engebretsen et al. (1996). Summary of the physical properties used in the experiments of both Medvedev et al. (1990) and Engebretsen et al. (1996) are listed in Table 1. It is apparent from Table 1 that both used granular filters in which the length ratio L/d_p and the porosity ε, were varied within similar ranges. Furthermore, both used similar incident shock wave Mach numbers. As could be expected the experimental results obtained by these authors, shown in Fig. 2, exhibited a similar tendency in the variations of the exit relative pressure behind the transmitted shock wave $\Delta P_{exit}/P_0$ as function of the filter length (here P_0, is the initial gas pressure inside the shock tube). However, while the results obtained by Medvedev et al. (1990) demonstrated a strong dependence of the exit relative overpressure on the shock wave Mach number M_s, those of Engebretsen et al. (1996), presented in Fig. 2 by a single dashed line, did not indicate a dependence of $\Delta P_{exit}/P_0$ on M_s. In addition, Engebretsen et al. (1996) stated that the effect of changing the material density and the size of the granules on the attenuation phenomenon was negligibly small. Such conclusion casts doubts because the particle size is responsible for the granular filter permeability, which has a direct effect on the shock wave attenuation. Another feature, which most probably affects the wave attenuation, is the duct geometry. For cases when the factor $H/d_p < 20$ (here H is the cross-section width of the channel), the side wall friction may strongly affect the flow (Munch-Andersen, 1983). As a result, one-dimensional presentation of the flow pattern inside a granular filter is questionable. The air-gap length downstream of the filter Δ,

Table 1
Experimental conditions in the shock tube studies

Particle type	Particle diameter, d_p (mm)	Filter porosity, ε	Filter length, L/d_p	Air gap length, Δ (mm)	Geometric factor, H/d_p	Shock wave strength, P_4/P_1 or M_s	Reference
Plastic spheres	10.00	$0.272 \div 0.38$	19	2800	12.50	$P_4/P_1 = 5 \div 20$	Engebretsen et al. (1996)
Glass spheres	15.52	$0.38 \div 0.41$	26	2800	8.05	$P_4/P_1 = 5 \div 20$	Engebretsen et al. (1996)
Polyethylene spheres	3.90	0.38	15	1000	10.26	$M_s = 1.15,\ 1.28,\ 1.47$	Medvedev et al. (1990)
Steel cylinders	10×12	0.41	16	1000	3.30	$M_s = 1.15,\ 1.28,\ 1.47$	Medvedev et al. (1990)
Porcelain spheres	15.8	0.44	10	1000	2.53	$M_{rms} = 1.15,\ 1.28,\ 1.47$	Medvedev et al. (1990)
Claydite spheres	21.9	0.50	11	1000	1.82	$M_s = 1.15,\ 1.28,\ 1.47$	Medvedev et al. (1990)

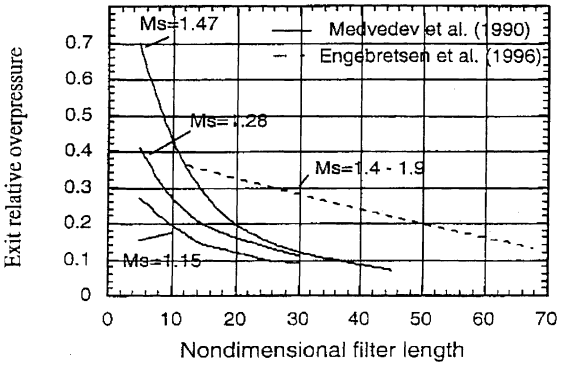

Fig. 2. Attenuation of shock waves during their propagation through granular filters. Nondimensional parameters used in this figure conform to those used by Medvedev et al. (1990). The exit relative overpressure is the ratio of the pressure behind the shock wave transmitted through the granular filter ΔP_{tranc} to the initial gas pressure $P_0 = 1$ bar, the nondimentional filter length is $\theta = 1.75(1-\varepsilon)L/\varepsilon d_p$.

may also affect the filter performance depending on how the filter is installed inside the duct, close to or far upstream of the protected surface (Gelfand et al. 1987). Since the air-gap length used by these authors was sufficiently large ($\Delta = 1 \div 2.8$ m), one cannot infer any practical information from their results regarding the role of this air gap in real ventilation systems.

Bearing these in mind, the main goal of the present study is to investigate the dependence of the granular filter performance on the following parameters:

- The filter length, L.
- The length of the air-gap downstream of the filter, Δ.
- The diameter of the beads composing the filter, d_p.
- The density of the beads composing the filter, ρ_p.
- The roughness of the side walls of the filter.

During the present study, we looked first at the dynamics of the pressure signature upstream of and inside the filter for different filter lengths and compositions. Thereafter, we checked the influence of the air-gap length on the obtained pressure signature. Finally, experiments were repeated to reveal new features, which arise when the filters were placed close to the protected surface (no air gap). The knowledge to be obtained from the present study should provide a basis for protection design not only for shelters and other high-priority military and urban assets, but also for combustion suppressors, protective shields for munitions storage facilities, etc. (Lind et al. 1999).

2. Experimental set-up

All the experiments were carried out in a vertical shock tube shown in Fig. 3. The tube is made of a 31 mm × 31 mm steel tube. The driver was filled with air at initial pressure of 0.6 ± 0.001 MPa and the air in the channel was at atmospheric pressure. A fast opening pneumatic valve having a rise-time of about 1 ms (ISTA, St. Petersburg, Russia) was installed between the driver and the channel in order to improve the repeatability of the post shock wave conditions. Some typical results, demonstrating the shock tube performance, are shown in Fig. 4. Results marked by (1) were obtained using the ISTA valve, results (2, 3) are experimental results of Kosing et al. (1999) obtained with a piston actuated valve. The solid line shows analytical results for $M_s = M_s(P_{41})$ As can be seen from this figure the Mach number values obtained while using the ISTA valve are the closest to the analytical prediction for $M_s < 1.6$. Note that in the present study all the tests are

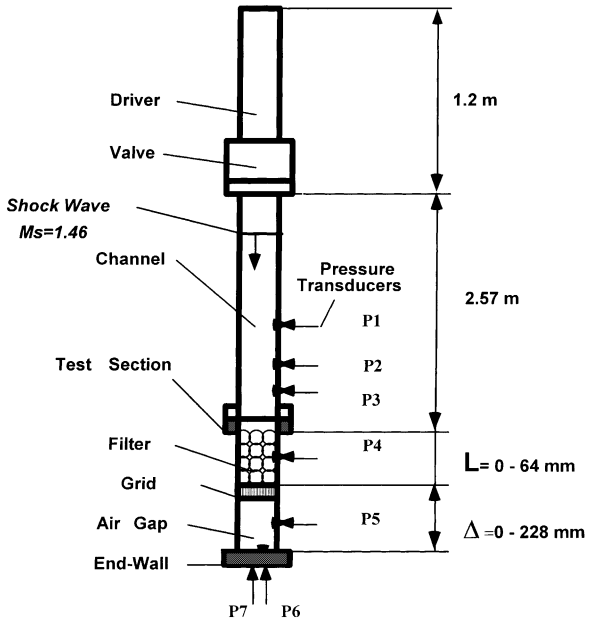

Fig. 3. Schematic description of the vertical shock tube used in the present experiments.

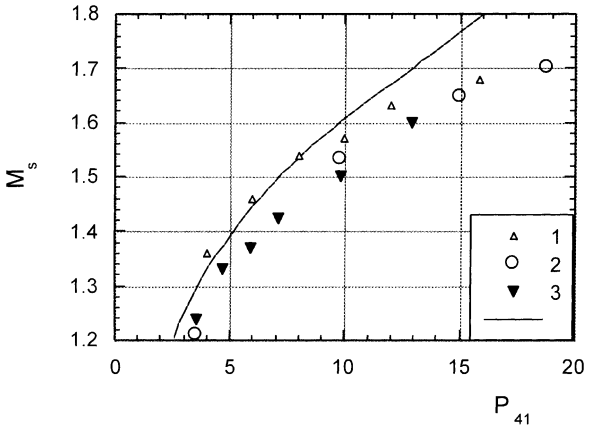

Fig. 4. Incident shock wave Mach number M_s vs. the pressure ratio $P_{41} = P_4/P_1$. P_4 is the driver pressure and P_1 is the channel pressure.

confined to a single incident shock wave Mach number, $M_s = 1.46 \pm 0.01$. In order to measure the shock wave propagation velocity and the overpressure behind the shock wave, the test sections were instrumented with 603H Kistler pressure transducers. Two of them (P4 and P7) were protected from having a direct contact with the solid particles by a screen permeable to the gas, these gauges measure the local gas pressure. The recorded data were stored using a data acquisition system Gage-Scope CS 220 with a sampling rate of 500 KHz per channel on an IBM-486 computer.

A rigid grid having an area ratio of 0.31 (ratio between the open to the total area), is placed above the test section end-wall and is used as a support for the granular filter. The length Δ of the air gap between the grid and the test section end-wall can easily be changed from 0 to 228 mm. The experimental procedure was as follows. First the test section was lifted off the holding flange at the rear end of the channel and the granular material used in earlier experiments was removed. Then, a new granular material was poured on the supporting grid from a funnel located directly above the apex of the test section. Since the bulk density depends on the agitation experienced by the particles during the discharge procedure, it was a good practice to keep the funnel at a constant height above the free surface of the granular bulk.

Special attention was given to ensure that the bulk free surface remained flat and normal to the test section sidewalls. Once the preparation procedure was completed, the thickness, L, of the granular filter was measured with an accuracy of about ± 1 mm and the test section was bolted. Summary of the main physical characteristics of the spherical particles used as filters is given in Table 2. Note that Rimax are ceramic granules of $ZrSiO_4$ produced by Rami Ceramic Industries (1991). Glass and steel beads are products of BioSpec. The values given for the particle density, ρ_s, in Table 2 are taken from the material quality certificate. All the materials were grated using a shaker and set of sieves with calibrated mesh sizes conforming to ASTM Standard. The values of the overall bulk volume, V_b, and its weight in air, m_b, were used to obtain the bulk density, ρ_b, the relative density ($\nu = \rho_b/\rho_s$) and thus, the porosity ($\varepsilon = 1 - \nu$) of the granular filter. Hereafter, each tested material will be identified, in the text and the figures, by the name of the material and the sieve code number or particle diameter, d_p, assigned to it in Table 2. It is clear from Table 2 that:

Table 2
Main physical characteristics of the granular materials used in the present study

Material	Particle diameter, d_p (mm)	Particle density, ρ_p (g/cm^3)	Filter length, L (mm)	Porosity, ε
Glass 8	2.4	2.5	8–63	0.38
Glass 18	1.0	2.5	5–63	0.40
Glass 35	0.5	2.5	4–27	0.39
Rimax 8	2.4	4.1	63	0.42
Rimax 18	1.0	4.1	63	0.35
Steel 5	4.4	7.7	4.4–22	0.49
Steel 10	2.0	7.7	12–63	0.39
Steel 14	1.4	7.7	16–46	0.40
Steel 18	1.0	7.7	4–49	0.35
Steel 35	0.5	7.7	6–26	0.40

1. While the porosity of the filters was almost constant large variations were observed in the particle diameter and its density.
2. The filter length was changed from $L = 6$ to 63 mm.
3. The air-gap length was changed from $\Delta = 0$ to 228 mm.

3. Physical model

A series of numerical calculations were performed employing a simple filtration model, which is described briefly in the following.

3.1. Assumptions

1. Both the gas and the solid phases are chemically inert.
2. The solid particles are uniformly distributed inside the granular bulk.
3. All the solid particles are of identical size and have spherical shape, which is maintained during the impact.
4. The gaseous phase behaves as a perfect gas.
5. The flow field is one-dimensional.
6. Correlations obtained for a steady flow through a packed bed can be used for treating the momentum and energy exchange between the gas and the solid phases.
7. The skeleton of the granular filter is treated as a rigid body.

3.2. The governing equations

Similar to Engebretsen et al. (1996) we treat the granular filter as a perforated plate having a length, L, and porosity, ε, that is equal to that of the real granular filters placed inside the shock tube. The conservation equations for mass, momentum and energy for the gas flowing through a tube with a perforated insertion can be written as follows (Gottlieb, 1986):

$$\frac{\partial \rho}{\partial t} + \frac{\partial(\rho V)}{\partial x} = -\frac{1}{A_x}\frac{\partial A_x}{\partial x}(\rho V), \tag{1}$$

$$\frac{\partial(\rho V)}{\partial t} + \frac{\partial(\rho V^2)}{\partial x} + \frac{\partial P}{\partial x} = -\frac{1}{A_x}\frac{\partial A_x}{\partial_x}(\rho V^2) + F_\mathrm{f} + F_\mathrm{h}, \tag{2}$$

$$\frac{\partial \rho(c_v T + \frac{1}{2}V^2)}{\partial t} + \frac{\partial\{\rho V(c_v T + \frac{1}{2}V^2 + P/\rho)\}}{\partial x} = -\frac{1}{A_x}\frac{\partial A_x}{\partial x}\rho V\left(c_v T + \frac{1}{2}V^2 + \frac{P}{\rho}\right) + Q, \tag{3}$$

$$\frac{\partial T_\mathrm{p}}{\partial t} = -\frac{Q\varepsilon}{\rho_\mathrm{p}(1-\varepsilon)c^*}, \tag{4}$$

$$P = \rho R T, \tag{5}$$

where A_x is the open cross-section area of the tube; F_f is the body force, resulting from the friction, per unit volume; $F_\mathrm{h} = -(\xi/L)(\rho V|V|/2)$ is the body force, resulting from the head losses, per unit volume due to the area change; ξ is the head losses coefficient, Q is the heat flux term; and c^* is the particle specific heat capacity. Other variables were defined earlier.

For the area change, $A_x(x)$, through the perforated plate Gottlieb (1986) suggested the following approximation:

$$A_x(x) = A_{x0}\mathrm{OAR}^{1/2}\exp\left[\ln\left(\frac{1}{\mathrm{OAR}^{1/2}}\right)\cos\left(2\pi\frac{x}{L}\right)\right], \tag{6}$$

where A_{x0} is a constant cross-section of the tube. From Eq. (6), one can obtain

$$\frac{1}{A_x}\frac{\partial A_x}{\partial x} = \frac{\pi}{L}\ln(\mathrm{OAR})\sin\left(2\pi\frac{\chi}{L}\right). \tag{7}$$

Here OAR is the plate open area ratio, which in the present case is equal to the filter porosity, ε, and χ is the local distance inside the granular filter $0 \leqslant \chi \leqslant L$. Note that for the present conditions, the value of the head loss coefficient is $\xi = 0$ (Gottlieb, 1986).

In order to account for the friction force and the heat transfer, the following well-known approximations were used (Rogg et al., 1985):

$$F_\mathrm{f} = -C\frac{\rho V|V|}{d_\mathrm{p}}\frac{(1-\varepsilon)}{\varepsilon}\left[\frac{180(1-\varepsilon)}{Re_\mathrm{p}} + 1.8\right], \tag{8}$$

$$Q = -6\frac{(1-\varepsilon)}{\varepsilon}\frac{\lambda Nu}{d_\mathrm{p}^2}(T - T_\mathrm{p}). \tag{9}$$

For Nusselt number (Nu) and gas viscosity (μ) the following correlations were used:

$$Nu = 2 + 0.8\,Re_\mathrm{p}^{0.7}\,Pr^{1/2}, \tag{10}$$

$$\mu = 1.71 \times 10^{-5} \times \left(\frac{T}{273}\right)^{0.73}. \tag{11}$$

In the system of equations (1)–(5), ρ, P, T, V are the gas density, pressure, temperature and the velocity; T_p is the particle temperature, μ and λ are the gas viscosity and the heat transfer coefficients and c_v is the gas specific heat capacity at constant volume. The porosity, ε, is equal to 1 everywhere excluding the granular bulk, where $\varepsilon = \text{const} < 1$ inside the granular bulk. R is the gas constant, $Re_p = \rho\varepsilon V d_p/\mu$ is the Reynolds number and $Pr = \mu c_p/\lambda$ is the Prandtl number. Notably, the constant $C = 1.25$ appearing in Eq. (8) is a single fitting parameter of the system of equations (1)–(3) which ensures good agreement between the experimental and the theoretical results throughout all the studied conditions.

The homogeneous system of equations (1)–(3) was solved numerically using a TVD scheme of second-order accuracy in time and in space. An operator splitting technique was employed for treating the source terms.

4. Results and discussions

The effect of the head-on collision of a planar shock wave with a granular filter on the post shock overpressure downstream of the filter was studied experimentally using two different experimental arrangement. In the first, the granular filter rested on a grid separated by an air gap from the end-wall. In the second, the granular filter was placed directly on the shock tube end-wall. The dimensional parameters affecting the considered flow are:

- The diameter of the spherical particles, d_p.
- The length of the granular filter, L.
- The length of the air gap, Δ.
- The peak overpressure behind the shock wave downstream, P_{trans}, and upstream, P_{inc}, of the filter.
- The end-wall matching time, t_m, which is the time passed from the moment the transmitted shock wave reached the test section end-wall until the moment the end-wall pressure reached a steady equilibrium level.

During the present study, these parameters were varied over a wide range resulting in a large body of data. The use of the following dimensionless parameters enabled, a clear presentation of the obtained results:

- The attenuation coefficient, K_a.
- The overpressures ratio between the transmitted and the incident shock waves:

$$K_a = P_{tranc}/P_{inc}.$$

- The matching time: $\bar{T} = t_m a_0/d_p$ (a_0 is the speed of sound in air at ambient conditions).
- The filter length: L/d_p.
- The air-gap length: $D = \Delta/d_p$.

Since the main interest is focused on the attenuation effect caused by the granular filter on the shock wave, the following key questions should be addressed:

1. Does the proposed physical model describe correctly the experimental findings for all the studied conditions?
2. How does the granular filter parameters affect the magnitude of the attenuation coefficient, K_a?
3. How does the end-wall matching time, $\bar{T}$, change with changes in the air-gap length, Δ?

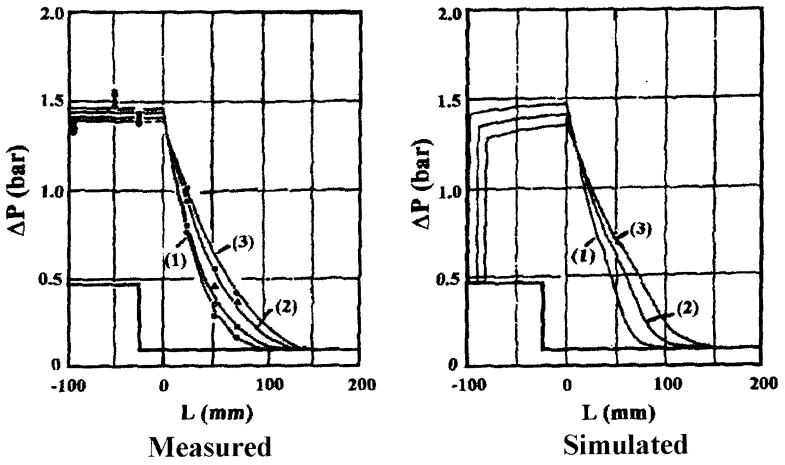

Fig. 5. Comparison between the experimental results of Rogg et al. (1985) and the present simulations.

Experimental and numerical results regarding the gas pressure distributions upstream of and inside the granular layer are given in Fig. 5. The results are for three different granular layers, all composed of glass beads. In the first (marked by 1 in Fig. 5) the beads diameter is $d_p = 4$ mm, in the second (marked as 2 in Fig. 5) $d_p = 6$ mm, and in the third $d_p = 8$ mm. It is clear from inspecting Fig. 5 that good agreement between the experimental results and the numerical predictions exists inside the filter while upstream of the filter the pressure field is not predicted correctly by the model.

4.1. The shock wave attenuation due to the presence of the grid

For assessing the shock wave attenuation due to the presence of a granular layer it is important to know what is the contribution of the grid, supporting the granular filter, to the shock wave attenuation. For answering this question experiments were conducted only with the presence of the grid inside the channel. The pressures were recorded again upstream and downstream of the grid (pressure transducers P3, P5 and P6 in Fig. 6). In the recorded and simulated pressure histories (also shown in Fig. 6) a few pressure jumps are seen. The first pressure jump, seen in the pressure traces recorded by gauges P3 and P5, is due to the passage of the incident and the transmitted shock waves at the measuring point. From these pressure jumps the attenuation coefficient, K_a, due to the grid presence could be evaluated. It was found to be $K_a = 0.75$. The second jump in the pressure traces is due to arrival of the reflected shock wave to the measuring points. Straight lines, indicating an x–t diagram for the transmitted and the reflected shock wave trajectories, were added to the recorded pressures shown in Fig. 6. It is apparent from this diagram that the trajectories of both the incident and the transmitted shock waves have the same slope. The same is true for the passage of the reflected shock wave, from the channel end-wall, through the grid. As expected all the reconstructed shock waves trajectories were straight. The series of small peaks observed in the pressure signature recorded by transducers P3 and P5 is a result of multiple shock wave reflections between the end-wall and the grid. Notably, an

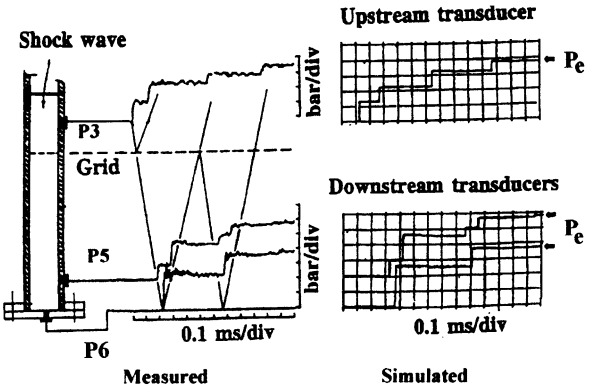

Fig. 6. Measured and calculated pressure histories upstream and downstream of the grid placed inside the channel.

equilibrium pressure P_e, at the end-wall, is actually reached even after the second peak at the pressure trace from transducer P6. This peak is due to the secondary shock wave origin, which was previously reflected at the grid (see the wave diagram in Fig. 6). Notably, in spite of the energy losses in the course of numerous shock wave reflections in the air gap, the final pressure, P_e, looks much the same or equal to the gas pressure, which would have been recorded at the end-wall had the incident shock wave been reflected directly from it. The time duration of $\approx$500 μs between the first and the second peaks at the pressure trace from transducer P6 is the time period which is required for the gas pressure to reach the equilibrium value, P_e, at the end-wall. We refer to this time period as the matching time, t_m.

In addition to illustrating the pressure histories and the shock wave trajectories, the net result of this figure is that the numerical model given by Eqs. (1)–(5) accurately predicts the pressure traces and the attenuation coefficient, K_a, when the grid is free from the granular filter.

4.2. Gas pressure histories inside the filter and at the end-wall

Examples of the recorded and the calculated pressure histories, at the location of pressure transducer P4 are shown in Fig. 7. This pressure acts on the sidewall of the granular filter. The considered filters are composed of 2.4-mm diameter glass spheres. Three different filters were tested; the first (1) had a length of 36 mm, the second (2) 50 mm, and the third (3) 64 mm. For all three lengths, the air gap between the filter and the end-wall was 106 mm long (in order to illustrate the repeatability of the measured results two experimental pressure readings obtained under similar conditions for each filter length, L, are reproduced in the left-hand side of this figure). It is evident from Fig. 7 that the presence of the filter affects the rate of the pressure build-up on the sidewall. The rate of the pressure build-up decreases with increasing the filter length. It is also apparent from Fig. 7 that during the covered test time the pressure inside the filter does not reach the equilibrium level, P_e. The longer the filter is, the slower is the quasi-steady pressure recorded by the sidewall transducer. A similar feature is also evident in the simulated pressure traces shown in Fig. 7. However, close inspection of these traces shows that the theory somewhat overestimates the final pressure for the shortest filter while it underestimates the final pressure for the longest one.

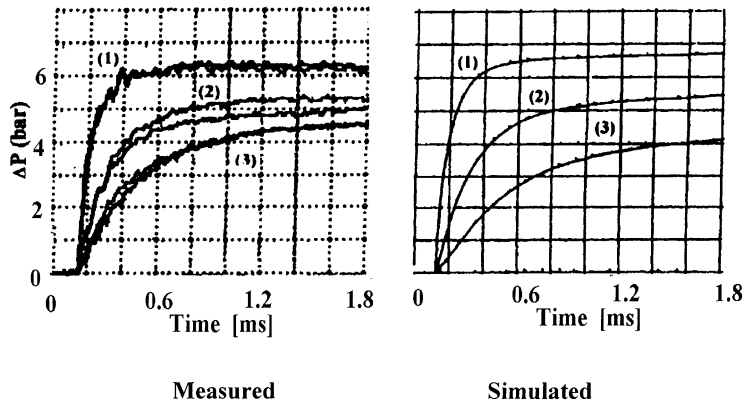

Fig. 7. Measured and simulated gas pressure histories inside granular filters composed of Rimax particles. Filters length are equal to: (1) $L = 6.5$ mm, (2) $L = 36$ mm, and (3) $L = 50$ mm. For all the experiments $d_p = 2.4$ mm.

The pressure history recorded by gauge P6, placed at the end-wall, is shown in Fig. 8. As could be expected, now a different pressure history is observed (compare Figs. 7 and 8). The first pressure jump experienced by the end-wall behind the reflected shock wave (in Fig. 8) is actually sensitive to the filter length and decreases with L (compare these signals with those shown in Fig. 6). Subsequent jumps in these traces, in similar to the previous case shown in Fig. 6, are caused by collisions between the transmitted shock wave with the end-wall and with the grid. The expected increase in the matching time associated with the increase in the filter length is also evident from Fig. 8. The filter presence weakens the transmitted shock wave and thus, the thicker the filter is, the slower the gas pressure reaches the equilibrium value P_e. Here too qualitative agreement is found between the simulated and the measured pressure traces. The best correlation is observed for the results obtained for the granular filter of minimal length (see curve 1) while for two other cases (shown by curves 2 and 3) with the longer filters the agreement between the experiment and the theory worsens. Given the complexity, this feature as well as other questions related to the range of validity of the model, and its limitations deserve further study.

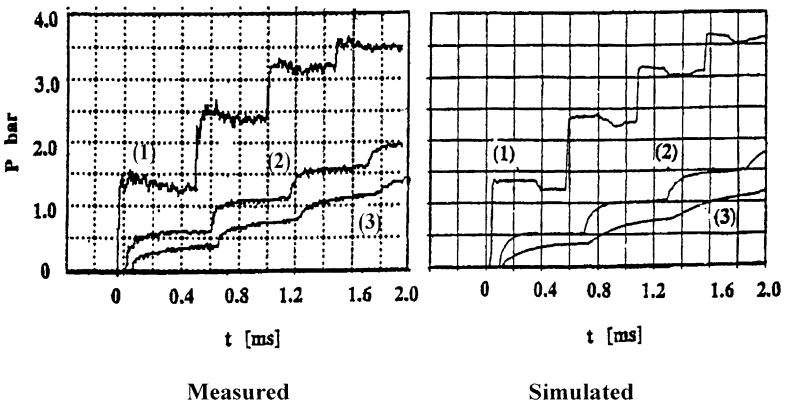

Fig. 8. The end-wall gas pressure build-up for different filter lengths: (1) 6, (2) 35 and (3) 64 mm. Glass spheres $d_p = 2.4$ mm, the air-gap length is $\Delta = 106$ mm.

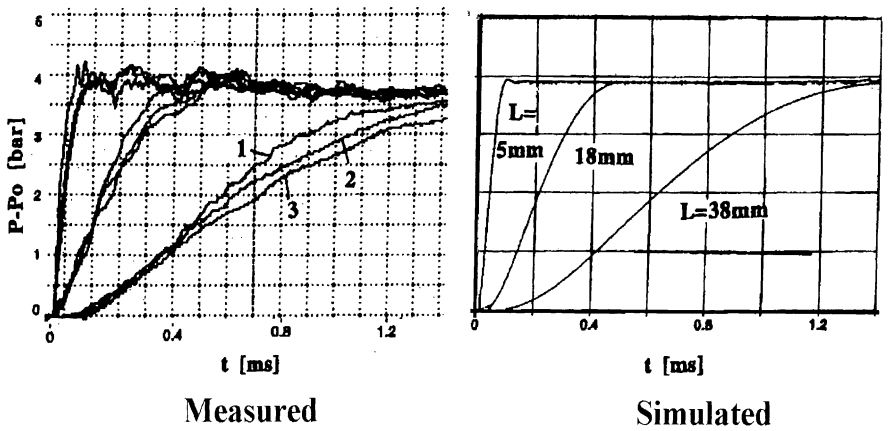

Fig. 9. The end-wall gas pressure traces for granular filters without an air gap. Experimental conditions: (1) steel particles, (2) glass beads. In both cases the test section walls were covered with sandpaper; (3) glass beads inside the test section covered with glass walls. For all the experiments $d_p = 0.5$ mm.

Next we consider the case when the granular filter is placed inside the shock tube directly over the end-wall, i.e., without an air gap. In this case, some of the particles composing the filter are in a direct contact with the end-wall and as a result the axial stress, generated by the transmitted shock wave, is acting on the walls of the test section. This gives rise to a proportional friction-drag and to a rearrangement of the particles. Because of the direct loading, the granular bulk would have higher resistance to the flow and the gas filtration at the end-wall would be more difficult. In order to assess the possible effect of the increased resistance to filtration following the shock wave impact, experiments were conducted with the following geometry. First, the test section was covered with a sand paper to increase significantly the sidewalls friction. Then the results were compared with those obtained when thin polished glass plates (minimum friction) covered the sidewalls. These experiments were repeated using granular filters composed of either glass or steel particles. The recorded end-wall gas pressure, shown in Fig. 9, did not show any dependency on the sidewall roughness or, on the particles material density. The small shift observed between traces (1)–(3), shown in Fig. 9, is most probably due to the different packing of the granular bulks in subsequent tests. The validity of this conclusion is supported by the simulated results obtained for the pressure histories shown in Fig. 9. Note that, for this case, the agreement between the experiments and the simulations is closer than those observed in Figs. 7 and 8. Although the reason for the agreement to be so close in this case deserves further study, one can suppose that this fact justifies by itself the exclusion of particle movement in the proposed physical model. However, it can be interpreted as being the result of the small sensitivity of the gas filtration to possible variation in the bed structure caused by the shock wave impact.

4.3. Parametric study

4.3.1. Granular filters with an air gap

Fig. 10 shows results obtained during the course of the present study in a non-dimensional way. For short filters ($L/d_p < 10$) the shock wave attenuation increases dramatically (small values for

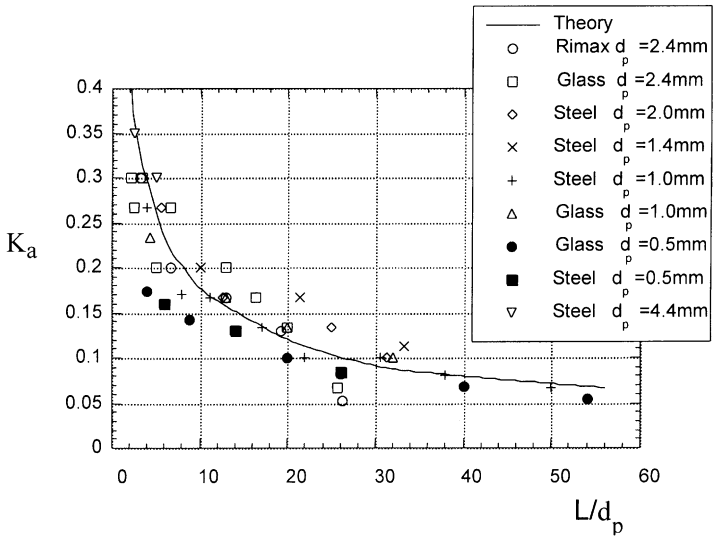

Fig. 10. The attenuation coefficient vs. the non-dimensional filter length.

K_a) with increase in the filter length. For longer filters $(L/d_p > 40)$ K_a approaches a constant value of $K_a \approx 0.05$. This trend is not surprising since the longer the filter is (or the smaller the particles are), the larger is the energy loss and thus the transmitted shock wave is more attenuated. It should also be noted that our numerical prediction (shown as a solid line in Fig. 10) represents the experimental findings well. Based upon this correlation it is of interest to compare the present results obtained for K_a with those of Medvedev et al. (1990) and Engebretsen et al. (1996), which were obtained under similar conditions. Fig. 11 contains a summary of these data. It is apparent that for the very short filters $(\theta \leqslant 15)$ good agreement is observed between the present results and Medvedev et al.'s (1990) curve fit. However for long filters, the present experimental results are closer to the curve fit of Engebretsen et al. (1996) whereas the data of Medvedev et al. (1990)

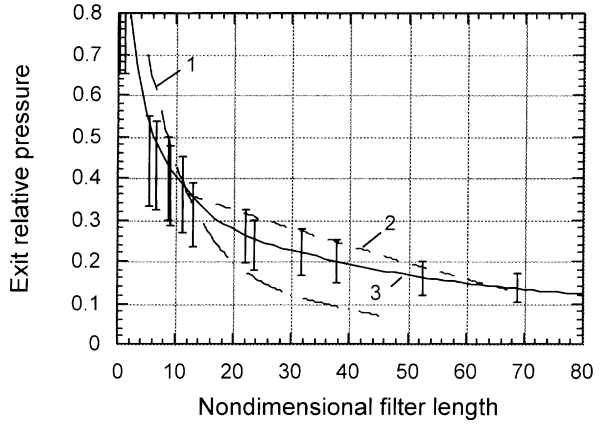

Fig. 11. Comparison between the experimental results of Medvedev et al. (1990) – line 1, Engebretsen et al. (1996) – line 2 and the present simulations – line 3, for incident shock wave Mach number $M_s = 1.47$.

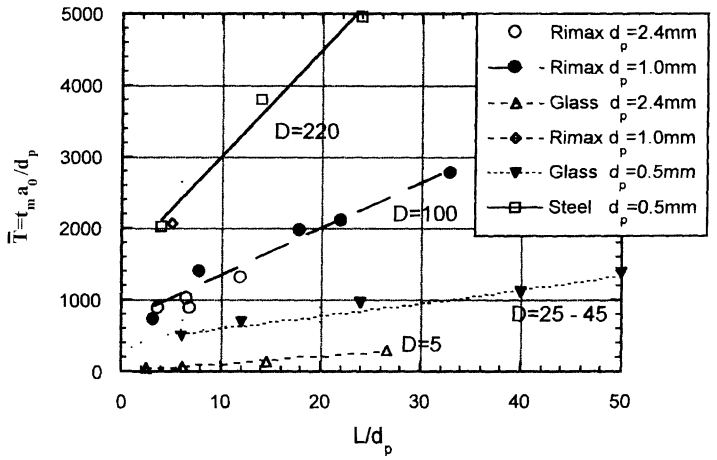

Fig. 12. The end-wall matching time vs. the filter non-dimensional length for different air-gap lengths $D = \Delta/d_p$.

indicate a monotonic decline. Results shown in Figs. 10 and 11 exhibit the attenuation of the transmitted shock wave due to the presence of a granular filter. They contain no information on the duration of the end-wall matching time. Information on the duration of the end-wall matching time is given in Fig. 12. From the curves and the experimental points, shown in Fig. 12, it could be concluded that filters composing of small particles result in slower pressure build-ups at the protected surface (end-wall in the present case). Similarly, the longer the granular filter is (or the longer is the distance between the filter and the protected surface), the larger is the end-wall matching time. Note that, since protected surfaces withstand more easily slower pressure build-ups in real protective systems, the matching time should be increased as much as possible. Thus, the particle dimension and both the filter length and the length of the air gap significantly affect the expected protection produced by the filter. On the other hand, the material composition of the filter (particle density) plays a minor role in increasing $\bar{T}$ or decreasing K_a.

4.3.2. Granular filters without an air gap

While for granular filters, which are followed by an air gap, the loading conditions are insensitive to the particle motion, it should not be the case for filters in direct contact with the protected surface. The most interesting result from such contact manifests itself by a large initial peak appearing in the total stress signals, like in those shown in Fig. 13. Gelfand et al. (1989) was probably among the first researchers who observed this peak in the experiments and established that, whereas, the peak duration was rather short (about 300 μs) it caused significant mechanical effects on the loaded surface. This effect was demonstrated in a special test case when an incident shock wave with an overpressure of 0.1 MPa impinged on a 0.1-mm thick copper diaphragm covered with a thin layer of powder. The impinging shock wave broke the diaphragm, while it did not break it when the diaphragm was not covered with powder. This feature was also the object of our previous studies (Britan et al., 1995; Ben-Dor et al., 1997; Britan et al., 1997a,b). It was clearly shown that during the shock wave impact on the filter surface the granular bulk is compressed and the end-wall promptly stops the particle motion. Hence this peak is caused by the particle rear-

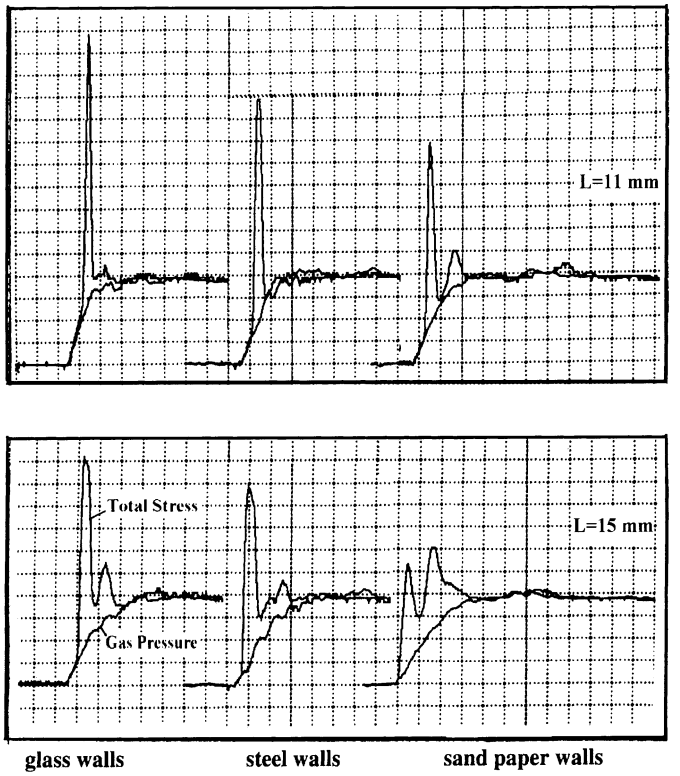

Fig. 13. Experimental pressure histories demonstrating the effect of the sidewall friction on the amplitude and the profile of the peak observed in the total stress. The filters are composed of 0.5 mm glass beads. Horizontal scale 0.1 ms/div; vertical scale 1 bar/div.

rangement inside the granular bulk, which in turn increases significantly the total stress exerted by the particles on the end-wall.

In an attempt to reduce the end-wall overloading, the main interest of the last series of experiments was centered on finding ways to hamper the particle motion during the shock wave impact. It seems reasonable to increase for this purpose the roughness of the walls containing the granular medium (particles). Results presented in Fig. 13 clearly show that in experiments with rough sidewalls (walls covered with sandpaper) the recorded peak in the total stress is significantly smaller than that recorded when using a test section having smooth glass sidewalls. It is also apparent from this figure that the sidewall roughness as well as the filter length have no practical effect on the final value of the gas pressure and the total stress. The filter length has an effect on the amplitude of the stress peaks. In fact, the thicker is the filter, the smaller the total stress peak becomes.

Another way to affect the particle motion during the shock wave impact is to use heavier particles and longer filters. An important conclusion related to this phenomenon can be drawn from the plot showing the amplitude of the total stress peak as a function of the filter length; (see Fig. 14). It is evident from this figure that while for filter lengths of $L < 34$ mm glass beads result in a higher peak than steel particles, for longer filters, $L > 34$ mm, the situation alters. It could

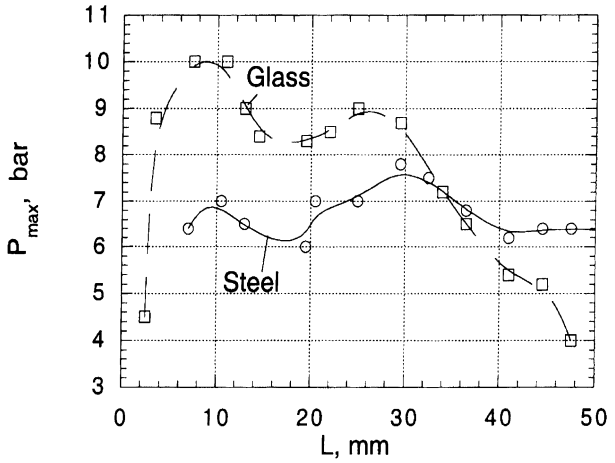

Fig. 14. The amplitudes of the total stress spike vs. the filter length. The filters are composed of 0.5-mm beads of steel or glass.

therefore be concluded that the complicated dependency of the total stress peak on the particle density deserves further studies.

Summary of the results relating the matching time for the end-wall gas pressure measurements and the simulations is shown in Fig. 15. It is apparent from this figure that there is a non-dimensional dependency between the filter length and matching time. Similar to the results shown earlier for the filters with an air gap, here too the longer the filter is (or the smaller the particles are), the longer is the matching time, $\bar{T}$.

In the present experimental findings the sidewall friction does not affect the end-wall matching time. Excellent agreement exists between the experimental and the numerical results (shown as a dashed line).

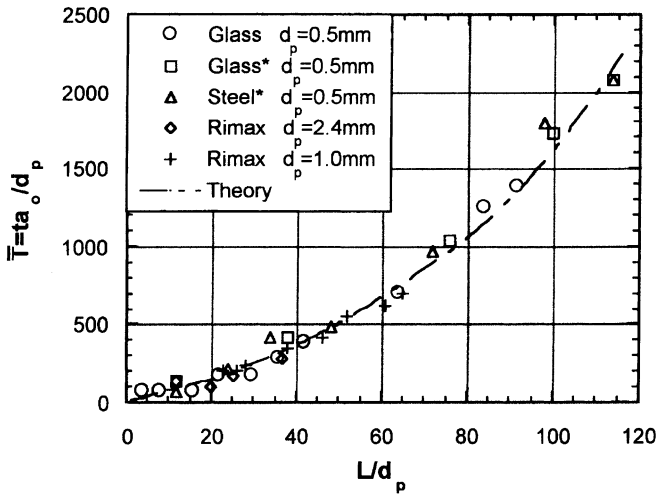

Fig. 15. The end-wall matching time vs. the filter length ($\Delta = 0$) for filters composed of different granular materials. A star superscript marks experimental points obtained while the test section sidewalls were covered with sand paper.

5. Summary and conclusion

Given the complexity of the physical problem being modeled, a comparison between the theory and the experiment is absolutely vital in order to clarify and understand the range of validity as well as the limitations of the physical model and the computer code. As the first step along this line the dominant parameters, namely the attenuation coefficient, K_a, and the matching time, $\bar{T}$ were specified to characterize the shock wave/granular filter interaction.

Two types of granular filters, with and without an air gap between the filter and the protected surface, were investigated. The main conclusions related to the performance of the granular filters are as follows.

1. The presence of an air gap between the granular filter and the protected surface prevents direct contact between the particles composing the granular filter and the protected surface. This eliminates peak pressure/stress on the protected surface. The amplitude of the transmitted shock wave at the filter exit decreases with an increase in the filter length or when the particle diameter decreases. Granular filters followed by an air gap result in an increase in the matching time. The matching time becomes longer when the length of the air gap increases or when the diameter of the particles composing the filter decreases. The particle density and the sidewall friction have no noticeable effect on the gas pressure downstream of the filter.

2. Granular filters without an air gap cause a peak in the total stress and thus the protected surface loading is enhanced as compared to the loading without a filter. The peak amplitude and its profile, in contrast to the equilibrium gas pressure, depend on the filter length, the particle density and the roughness of the sidewalls. The filter length and the particle diameter are the dominant factors also for the end-wall matching time.

3. The experimental findings were compared with numerical predictions based on a simple one-dimensional filtration model. While the agreement between the experiment and the simulations was mostly qualitative, the physical model correctly predicted the main details of the gas flow pattern affecting the attenuation coefficient, K_a, and the matching time, $\bar{T}$. A better quantitative agreement requires an improvement of the physical model. In a numerical computation, the gas pressure profiles as well as the times of arrival of the shock wave in the measurement ports placed upstream of, inside and downstream of the granular filter should be adequately resolved. This work is now in progress.

Acknowledgements

The authors would like to thank Professor D.M.J. Smeulders for valuable discussions. We acknowledge the support of the R&D Unit, Ministry of Defenses under Grant No. 85766201.

References

Ben-Dor, G., Britan, A., Elperin, T., Igra, O., Jiang, J.P., 1997. Experimental investigation of the interaction between weak shock waves and granular layers. Exp. Fluids 22, 432–443.

Britan, A., Elperin, T., Igra, O., Jiang J.P., 1995. Head-on collision of a planar shock wave with a granular layer. In: Schmidt, S.C., Tao, W.C. (Eds.), Proceedings of the ISCCM Conference, Part. 2, Seattle, WA, USA, pp. 971–974.

Britan, A., Ben-Dor, G., Elperin, T., Igra, O., Jiang, J.P., 1997a. Mechanism of compressive stress formation during weak shock waves impact with granular materials. Exp. Fluids 22, 507–518.

Britan, A., Ben-Dor, G., Elperin, T., Igra, O., Jiang, J.P., 1997b. Gas filtration during the impact of weak shock waves on granular layers. Int. J. Multiphase Flow 23, 473–491.

Engebretsen, T., Bakken, J., Hansen, E.W.M., Lysberg, I., 1996. Shock waves and gas flow through granular materials. In: Proceedings of the Workshop on Explosion Effects in Granular Materials, Oslo, pp. 111–131.

Gelfand, B.E., Medvedev, S.P., Borisov, A.A., Polenov, A., Frolov, S.M., Tsyganov, S.A., 1989. Shock loading of stratified dusty system. Combustion 9 (1/4), 153–165.

Gelfand, B.E., Medvedev, S.P., Polenov, A.N., Tsyganov, S.A., 1987. Interaction of non-stationary pressure waves with perforated partitions. Arch. Combust. 7 (1–2), 215–223.

Gottlieb, J.J., 1986. Lecture course notes on random-choice method for solving one-dimensional unsteady flows in ducts, shock tubes and blast-wave simulators, University of Toronto, Canada.

Kosing, O.E., Barbosa, F.J., Skews, B.W., 1999. A new, friction controlled, piston actuated diaphragmless shock tube driver. Shock Waves 9, 69–72.

Lind, C.A., Cybyk, B.Z., Boris, J.P., 1999. Attenuation of shocks: high reynolds number porous flows. In: The 22nd International Symposium on Shock Waves. Book of Abstract, London, p. 272.

Medvedev, S.P., Frolov, S.M., Gelfand, B.E., 1990. Shock wave attenuation by granular materials. Eng. Phys. J. (USSR) 55 (6), 924–928 (in Russian).

Mori, Y., Hijikato, K., Shimizu, T., 1975. Attenuation of shock wave by multi-orrifice. In: Proceedings of the 10th International Symposium on Shock Tube, Kyoto, pp. 400–407.

Munch-Andersen, J., 1983. Scale errors in model silo tests. In: Proceedings of the Second International Conference on Design Silos Strength and Flow, Stanford upon Avon, pp. 230–241.

Rogg, B., Hermann, D., Adomait, G., 1985. Shock-induced flow in regular arrays of cylinders and packed beds. Int. J. Heat Mass Transfer 28, 2285–2297.

Tong, K.O., Knight, C.J., Srivastava, B.N., 1980. Interaction of weak shock waves with screens and honeycombs. AIAA J. 18, 1298–1305.